Proc. of the International Conference on Mechanochemistry and Mechanical Alloying, Kraków, Poland, June 22–26, 2014

Microstructure Evolution of Tungsten-Based ODS Alloys Reinforced with the γ(Ni, Fe) Phase by a Secondary Ball Milling Method

C.-L. Chen*, Y. Zeng and J.-G. Lee
Department of Materials Science and Engineering, National Dong Hwa University,
No. 1, Sec. 2, Da Hsueh Rd., Shoufeng, Hualien 97401, Taiwan

In the current study, W-5Ni-2Fe-Y_2O_3 model alloys were produced using a high-energy planetary ball mill. The presence of the γ(Ni, Fe) phase is favored with respect to material properties in this alloy. Therefore, a secondary ball milling method was introduced to obtain a fine and uniformly distributed γ(Ni, Fe) phase. Phase development of mechanical alloyed powders was investigated by X-ray diffraction. The results show that the formation of the γ(Ni, Fe) phase was found after 18 h of a pre-milling procedure. A further secondary milling method produced a uniform microstructure with grain refinement. TEM results also show changes in the lattice parameters of the tungsten and γ(Ni, Fe) phase associated with the solid solubility limits in the alloy produced by secondary ball milling.

DOI: 10.12693/APhysPolA.126.907
PACS: 81.20.Ev, 81.20.Wk, 81.07.Bc, 81.05.Ni

1. Introduction

Oxide dispersion strengthened (ODS) tungsten heavy alloys have been developed as materials offering superior strength at elevated temperature and improving ductile to brittle fracture and the self-sharpening behavior of tungsten heavy alloys [1–3]. These special properties can be attributed to a uniform distribution of oxide dispersoids, which impede the movement of dislocations and retard recovery and recrystallization processes [4–7]. The ODS alloys were normally produced by mechanical alloying, which is a solid-state powder metallurgy processing technique that involves repeated cold welding, fracturing and rewelding of powder particles. The mechanical alloying of tungsten heavy alloys has been the subject of many studies [8–10]. A wide range of operating parameters has been investigated such as the milling atmosphere, the process control agent (PCA) and grinding media materials [11–14].

During the mechanical alloying process, formation of different intermetallic compounds can result in a significant effect on microstructural development and material properties. In heavy tungsten alloys, the addition of small amounts of Ni, Fe elements in a tungsten matrix promote liquid phase sintering and the binder phase γ(Ni, Fe) is normally formed between tungsten grains after sintering. This phase plays an important role in determining material properties, particularly in the densification and the improvement of the ductility of the alloy [8,9]. Therefore, in this work, in order to produce a large amount of the γ(Ni, Fe) phase with a uniform and refined structure, the standard procedure of fabrication of ODS tungsten alloys by mechanical alloying has been modified. A secondary ball milling method was introduced to synthesize tungsten-based ODS alloys reinforced with the γ(Ni, Fe) phase and to achieve a refined and homogeneous microstructure.

2. Experimental procedure

The material used in the present study has composition W-5Ni-2Fe-0.3Y_2O_3 (in weight percent). Initially, the elemental powders of nickel and iron were pre-milled for different periods: 0, 6, 12, 18, and 24 h to investigate the formation of the γ(Ni, Fe) phase analyzed by X-ray diffraction (XRD). The pre-milled powders of the Ni-Fe alloy system for 24 h of milling were then further secondarily ball milled with tungsten powders and Y_2O_3 nano-oxide particles for additional 18 h to achieve homogeneity and refinement of the γ(Ni, Fe) phase distributed in the tungsten matrix. The milling procedure mentioned above named as "secondary milling" is applied in this work. In addition, a standard milling procedure was used for comparison. All different powders of tungsten, nickel and iron with nano-oxide particles were milled for 36 h. In this case, we named this procedure as "primary milling". The mechanical alloying process was performed in an argon atmosphere using a planetary ball mill (Retsch PM 100). Milling experiments were carried out using a tungsten carbide grinding medium with a ball to powder ratio of 10:1. The powders were loaded and sealed in a glove box protected by a highly purified argon atmosphere to avoid oxidation. The mechanically alloyed powders were then sintered in a mixed hydrogen–argon atmosphere at 1400 °C for 30 min. The formation of the γ(Ni, Fe) phase during pre-milling and phase characterization of the synthesized powders were conducted using X'PERT PRO XRD with Cu K_α radiation. The crystallite size and lattice strain was estimated using Scherrer's formula as

*corresponding author; e-mail: chunliang@mail.ndhu.edu.tw

follows [15]:

$$B_{\mathrm{r}} = \frac{0.9\lambda}{t\cos\theta} + \eta\tan\theta, \tag{1}$$

where B_{r} is the total broadening due to crystal refining and lattice strains, λ is the X-ray wavelength, t is the crystallite size, θ is the Bragg angle and η is the strain in the material. The microstructure of the milled powders and sintered specimens was examined using a JEOL JSM-7000F field-effect scanning electron microscopy (FE-SEM) and FEI Tecnai F20 G2 Field Emission Gun transmission electron microscopy (TEM).

3. Results and discussion

3.1. Microstructural observations during ball milling

Figure 1 displays an SEM image morphology of powder particles during the milling process after various times The morphology of the Ni, Fe powders pre-milled for 24 h are shown in Fig. 1A. A composite microstructure consisting of cold welded γ(Ni, Fe) solid solution phase is formed as a result of repeated cold welding and fracturing of powder particles. In this stage, a fine particle of the γ(Ni, Fe) phase can be achieved after a long milling duration. Figure 1B,C shows the morphological evolution of the tungsten and pre-milling of the γ(Ni, Fe) powder particles milled for different times (6, 12, and 18 h). This procedure was named earlier as secondary ball milling. A number of agglomerates with non-uniform morphology particle are formed after 6 h of milling, see Fig. 1B, as a result of cold welding and plastic deformation of the tungsten and γ(Ni, Fe) powders. Further milling to 12 h caused a significant decrease in particle size and the particles with a flake-like or platelet-like shape were also observed in Fig. 1C. By increasing the milling time up to 18 h, see Fig. 1D, the particle size can be further refined and the morphology changes approximately into spherical shapes.

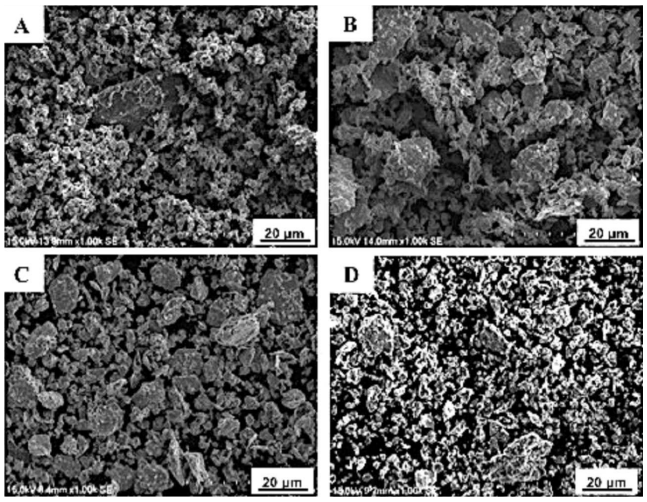

Fig. 1. SEM micrographs of Ni-Fe powders pre-milled for (A) 24 h and W–γ(Ni, Fe) powders milled for (B) 6 h, (C) 12 h and (D) 18 h.

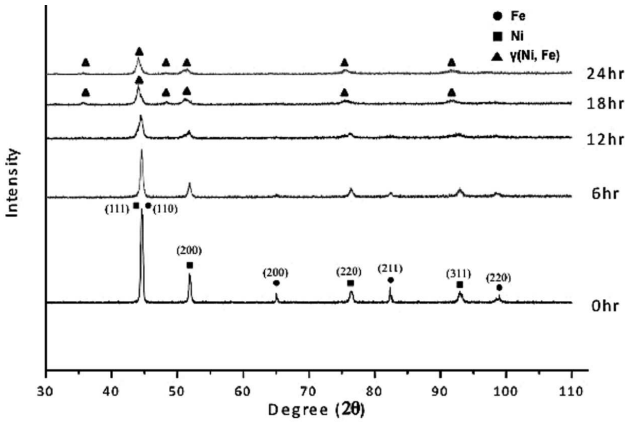

Fig. 2. XRD spectra of Ni-Fe powders milled for different milling durations: 0, 6, 12, 18, and 24 h.

3.2. Phase development of mechanical alloyed powders

Figure 2 shows the evolution of XRD patterns for pre-milled Ni-Fe samples as a function of milling time. The non-milled powder indicates the reflections corresponding to face centered cubic (fcc) Ni and body centered cubic (bcc) Fe. It is clear to observe that the iron reflection peaks of (200) and (211) disappear after 18 h of milling and the Ni peaks slightly shift towards lower angles. The results suggest that Fe atoms dissolve into the Ni crystalline lattice and expand the lattice on the Ni-Fe alloy system during ball milling, which promote the formation of a solid solution γ(Ni, Fe) phase. Figure 3 also shows the change in the crystallite size and lattice strain as a function of the milling time of the Ni, Fe powders. It is seen that the crystallite size decreased significantly after the first 12 h of milling and then began to steadily decrease up to a milling time of 24 h. However, the internal strain initially increases significantly with an increase in milling time. The results imply that the mechanical alloying process not only refines the powder but also increases the dislocations in the powder crystals. Additionally, the atomic diffusivity is promoted through a large amount of structural defects which enhanced the solid solution reactions of the γ(Ni, Fe) phase.

Figure 4 shows the XRD patterns of the W- γ(Ni, Fe) powders milled by the secondary milling method as a function of milling time. The non-milled powder indicates the diffraction peaks of the pure tungsten and the weak peaks of the γ(Ni, Fe) phase in the (111) and (200) directions The (111) peak of the γ(Ni, Fe) phase is still visible after 18 h of milling but it is less intense, suggesting that the γ(Ni, Fe) phase formed by the primary milling process might be difficult to dissolve back into the tungsten powder matrix. In addition, all diffraction peaks of tungsten become broader and weaker with increasing milling time, indicating a decrease in the crystallite size and an increase in the lattice strain. XRD measurements of the primary milled powder are also presented in Fig. 5 for comparison.

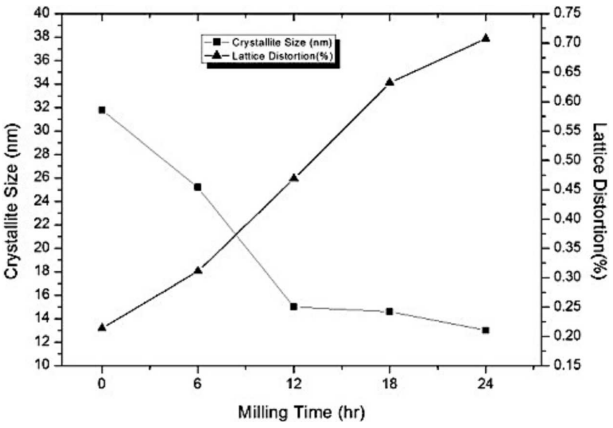

Fig. 3. Crystallite size and lattice distortion of the Ni-Fe powders milled as a function of milling time.

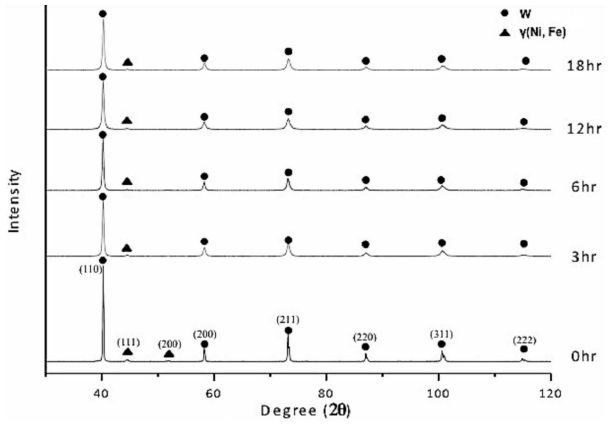

Fig. 4. XRD spectra of the secondary milled powders for different milling durations: 0, 3, 6, 12, and 18 h.

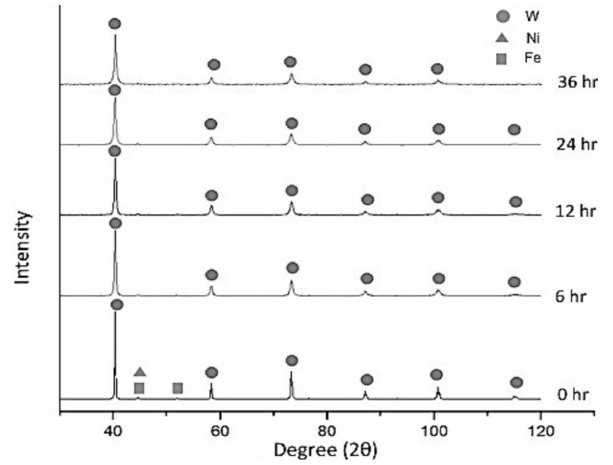

Fig. 5. XRD spectra of the primary milled powders for different milling durations: 0, 6, 12, 24, and 36 h.

3.3. Characterization of the sintered model alloys

3.3.1. SEM

Figure 6 shows the microstructure of the sintered model alloys using the primary milling and secondary milling methods. A non-uniform microstructure with a large size of the γ(Ni, Fe) phase was found in the primary milling sample, see Fig. 6A. The γ(Ni, Fe) phases precipitate at grain boundaries and this is confirmed by energy dispersive X-ray (EDX) spectroscopy. However, the microstructure of the secondary milling sample, see Fig. 6B, was found to consist of a uniform matrix with a large amount of the secondary γ(Ni, Fe) phase, which is considerably refined. The results can be attributed to the formation of the γ(Ni, Fe) phase caused by the secondary milling which is hard to dissolve back into the tungsten matrix during the secondary ball milling procedure. In this case, with continued milling, the second phase can be refined and a more homogeneous microstructure and distribution is produced.

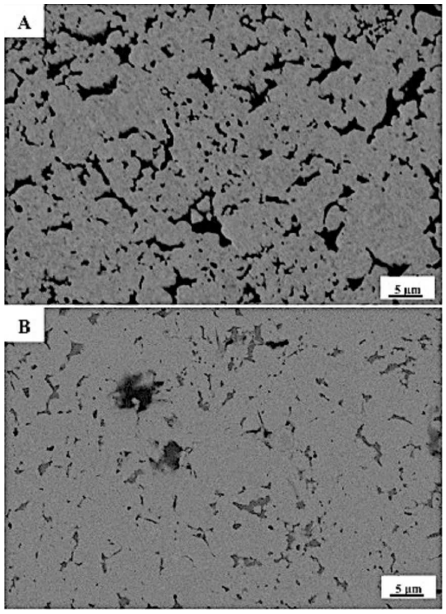

Fig. 6. SEM images of the sintered samples using (A) the primary milling and (B) secondary milling methods.

3.3.2. TEM

Figure 7A shows the bright-field TEM micrograph of the sintered model alloy with the primary ball milling procedure and the γ(Ni, Fe) phase was found to form between the tungsten grains. The use of a primary milling method provides a rapid transport path allowing the Ni, Fe elements to diffuse more rapidly into the tungsten matrix and thus the solubility of the alloy system can be extended, leading to an increase in the lattice parameters. Figure 7B displays the selected area diffraction (SAD) patterns of the γ(Ni, Fe) phase along the zone axis of [101] which had an average lattice parameter of 3.663 Å. Additionally, the (SAD) pattern of tungsten matrix,

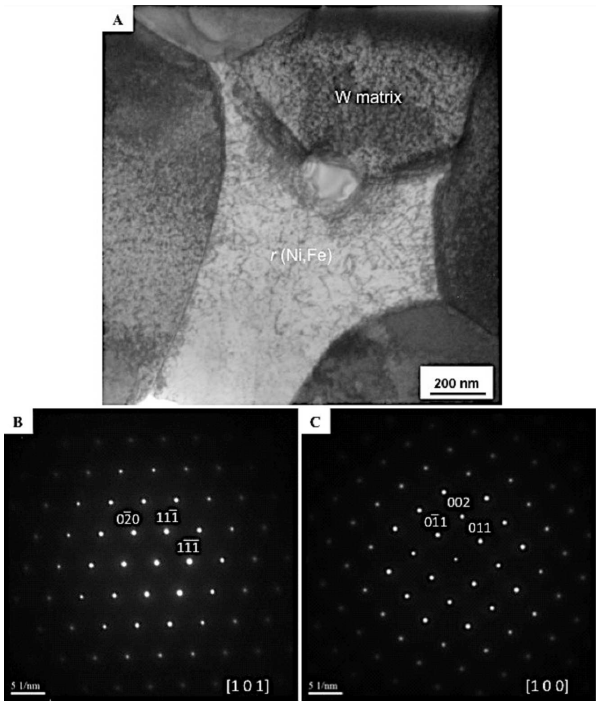

Fig. 7. The TEM investigation of the sintered samples using the primary milling: (A) the bright field image and (B, C) the SAD pattern of tungsten and the γ(Ni, Fe) phase.

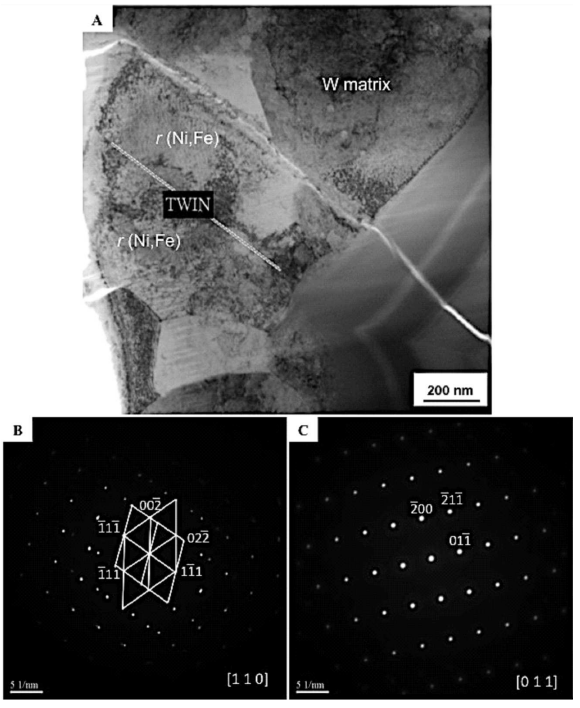

Fig. 8. The TEM investigation of the sintered samples using the secondary milling: (A) the bright field image and (B, C) the SAD pattern of the tungsten and γ(Ni, Fe).

see Fig. 7C, demonstrates the phase along the [100] zone axis with an average lattice parameter of 3.215 Å. The values obtained from experiments are greater than that of reference data ($a = .598$ Å for γ (Ni, Fe) and $a = 3.165$ Å for tungsten), suggesting that Ni and Fe were dissolved in the tungsten phase during sintering. Conversely, Fig. 8A shows the TEM image of the sintered model alloy with the secondary ball milling method. The twinned structure was observed in the γ(Ni,Fe) phase and suggests that the secondary milling procedure encourages a large strain deformation of the γ(Ni, Fe) phase and thus promotes the defect nucleation sites for deformation twins. This is well known as deformation-induced twinning [16].

In the present work, the secondary milling was the preferred mode of deformation for formation of the twinned crystal structure. In addition, Fig. 8B shows the SAD pattern of the twinned γ(Ni, Fe) phase along the zone axis of [110] and has an average lattice parameter of 3.610 Å. The tungsten phase is oriented along the [100] zone axis with an average lattice parameter of 3.179 Å, as shown in Fig. 8C. The measured lattice parameters were found to be consistent with reference values. This indicates that under secondary milling the formation of the γ(Ni, Fe) phase would lead to a limited solubility in the alloy system. In this case, the Ni, Fe elements are likely to be rejected from supersaturated tungsten solid solution matrix.

4. Conclusions

In this paper, a secondary ball milling method has been applied to synthesize tungsten-based ODS alloys reinforced with the γ(Ni, Fe) phase to achieve desired structure and properties. The XRD patterns of pre-milled Ni-Fe powders revealed that iron reflection peaks of (200) and (211) disappear after 12 h of milling. The Ni peaks slightly shift towards lower angles, indicating the formation of a solid solution γ(Ni, Fe) phase. A uniform matrix with a large amount of a fine γ(Ni, Fe) phase was obtained in the secondary ball milling sample. TEM examination also revealed that the use of a primary milling method provides a rapid transport path allowing the Ni and Fe elements to diffuse more rapidly into the tungsten matrix and thus the solubility of the alloy system can be extended, leading to an increase in the lattice parameters. However, the Ni, Fe elements are likely to be rejected from the supersaturated tungsten solid solution matrix during the secondary milling. Therefore, the γ(Ni, Fe) phase has a limited solubility in the alloy system. With continued secondary milling, the second phase can be refined and a more homogeneous microstructure is produced.

Acknowledgments

The authors would like to gratefully acknowledge financial support from the National Science Council of Taiwan under the grant NSC 102-2221-E-259-006.

References

[1] K.H. Lee, S.I. Cha, H.J. Ryu, S.H. Hong, *Mater. Sci. Eng. A* **458**, 323 (2007).

[2] J. Martínez, B. Savoini, M.A. Monge, A. Mñoz, R. Parej, *Fus. Eng. Des.* **86**, 2534 (2011).

[3] K.H. Lee, S.I. Cha, H.J. Ryu, M.F. Dilmore, S.H. Hong, *J. Alloys Comp.* **434–435**, 433 (2007).

[4] C.-L. Chen, P. Wang, G.J. Tatlock, *Mater. High Temper.* **26**, 299 (2009).

[5] C-L. Chen, G. J. Tatlock, A.R. Jones, *J. Alloys Comp.* **504**, S460 (2010).

[6] C-L. Chen, G.J. Tatlock, A.R. Jones, *J. Microsc.* **233**, 474 (2009).

[7] C. Suryanarayana, *Prog. Mater. Sci.* **46**, 1 (2001).

[8] C-L. Chen, C.-L. Huang, *Int. J. Refract. Met. Hard Mater.* **44**, 19 (2014).

[9] C-L. Chen, C.-L. Huang, *Intermetallics* **41**, 10 (2014).

[10] C-L. Chen, C.-L. Huang *Met. Mater. Int.* **19**, 1047 (2013).

[11] C.-L. Chen, Y.-M. Dong, *Mater. Sci. Eng. A* **528**, 8374 (2011).

[12] X.L. Wang, G.F. Wang, K.F. Zhang, *Mater. Sci. Eng. A* **527**, 3253 (2010).

[13] R. Júarez, J.J. Sũnol, R. Berlanga, J. Bonastre, L. Escoda, *J. Alloys Comp.* **434-435**, 472 (2007).

[14] Z. Oksiuta, N. Baluc, *J. Nucl. Mater* **386–388**, 426 (2009).

[15] C. Suryanarayana, *Norton MG. X-Ray Diffraction: A Practical Approach*, Plenum Press, New York 1998.

[16] C.X. Huang, K. Wang, S.D. Wu, Z.F. Zhang, G.Y. Li, S.X. Li, *Acta Mater.* **655–665**, 54 (2006).